# NanoSIMS imaging of D/H ratios on FIB sections

Dan Lévy, Jérôme Aléon, Alice Aléon-Toppani, David Troadec, Rémi
Duhamel, Adriana Gonzalez-Cano, Hélène Bureau, Hicham Khodja

## HAL Id: cea-02300872
## https://cea.hal.science/cea-02300872

Submitted on 30 Sep 2019

# NanoSIMS imaging of D/H ratios on FIB sections

Dan Lévy[1,2], Jérôme Aléon[1], Alice Aléon-Toppani[2], David Troadec[3], Rémi Duhamel[1], Adriana Gonzalez-Cano[1*], Hélène Bureau[1], Hicham Khodja[4]

[1] Institut de Minéralogie de Physique des Matériaux, de Minéralogie et de Cosmochimie (IMPMC), Museum National d'Histoire Naturelle, Sorbonne Universités, UMR CNRS 7590, 61 rue Buffon, 75005 Paris, France

[2] Institut d'Astrophysique Spatiale (IAS), University of Paris Saclay, 91405 Orsay, France

[3] Institut d'Electronique Microélectronique et Nanotechnologie (IEMN), CNRS, University of Lille, Avenue Poincaré, 59652 Villeneuve d'Ascq, France

[4] LEEL, NIMBE, CEA, CNRS, Université Paris-Saclay, CEA Saclay 91191 Gif sur Yvette Cedex, France

**ABSTRACT:** The D/H ratio imaging of weakly hydrated minerals prepared as Focused Ion Beam (FIB) sections is developed in order to combine isotopic imaging by Nanoscale Secondary Ion Mass Spectrometry (NanoSIMS) of micrometer-sized grains with other nanoscale imaging techniques, such as Transmission Electron Microscopy. In order to maximize the accuracy, sensitivity, precision and reproducibility of D/H ratios at the micrometer-size, while minimizing the surface contamination at the same time, we explored all instrumental parameters known to influence the measurement of D/H ratios in situ. Optimal conditions were found to be obtained with the use of (i) a $Cs^+$ ion source and detection of $H^-$ and $D^-$ at low mass resolving power, (ii) a primary beam intensity of 100 pA, and (iii) raster sizes in the range 8-15 μm. Nominally anhydrous minerals were used to evaluate the detection limits and indicate a surface contamination level of about 200 ppm equivalent $H_2O$ in these conditions. With the high primary intensity used here, the dwell time is not a parameter as critical as found in previous studies and a dwell time of 1 ms/px is used to minimize dynamic contamination during analysis. Analysis of FIB sections was found to reduce significantly static contamination due to sample preparation and improved accuracy compared to using polished sections embedded not only in epoxy but in indium as well. On amphiboles, the typical overall uncertainty including reproducibility is about 20 ‰ on bulk FIB sections and about 50 ‰ at the 1.5 μm scale using image processing (1σ).

## INTRODUCTION

Nanoscale Secondary Ion Mass Spectrometry (NanoSIMS) is a powerful technique for the surface analysis of trace elements and isotopes in materials, potentially allowing coupling with many other analytical techniques. One decade after its development[1,2], NanoSIMS analysis was used to image electron transparent sections prepared by Focused Ion Beam (FIB) in order to compare isotopic / trace element composition with mineralogy, as determined by Transmission Electron Microscopy (TEM). Most studies focused on oxygen, nitrogen and carbon isotopic systems, all elements having large ion yields in SIMS, which in turn allowed high lateral resolution imaging[3–6]. To our knowledge, only one study reported hydrogen isotopic analysis of FIB sections of organic material[7]. These measurements had several limitations: they were restricted to the mapping of large isotopic variations such as anomalies in meteorites[4,5,7], labelled biological material[3,6], or to elemental imaging[8]. Importantly, isotopic imaging was always performed after TEM, which required a complete initial characterization of the sections and did not allow specific analysis of sub-areas revealed as interesting from isotopic imaging. Furthermore, most of these studies did not use standards measured identically in FIB section, thus preventing precise quantitative measurements, since NanoSIMS analysis is very sensitive to surface conditions. Because the H isotopic composition is a well established geochemical tracer in many fields including biology[9,10], geology[11–13], astrophysics[14–17] and environment[18,19], the goal of the present study is to quantitatively image D/H ratio in FIB sections, with a precision allowing to resolve moderate isotopic variations.

A major difficulty in imaging D/H ratio in SIMS resides in the ubiquitous presence of water molecules that stick to the surface and create an hydrogen background[20,21]. This contamination is the result of two types of processes, which we refer to as (i) static contamination and (ii) dynamic contamination. All contamination sources independent from analysis are referred to here as static contamination, i.e. contamination resulting from sample degassing, atmospheric water adsorbed on the sample surface or residual water pressure in the analysis chamber. Dynamic contamination is considered here to correspond to all processes taking place in the analysis chamber during analysis. This includes for instance migration of water molecules at the sample surface into the sputtered area, arrival of water molecules impinging the sample surface from the residual gas, or redeposition of sputtered H atoms from the sample. Dynamic contamination clearly depends on static contamination but can be addressed by optimizing the measurement conditions, whereas static contamination needs to be taken care of prior to analysis (e.g. sample preparation, instrument vacuum).

Many attempts have been done to lower this hydrogen background but concluded that it is not possible to totally get rid of it[21]. This is the reason why most studies focus either on high lateral resolution imaging of D/H ratios in hydrogen-rich materials such as clays or organics[22,23], or measurement of the H/Si ratio in samples with low H content such as Nominally Anhydrous Minerals (NAMs) without imaging[24]. The present

study focuses on imaging D/H ratio in FIB sections of minerals having an hydrogen content intermediate between highly hydrated minerals and NAMs and will use amphiboles as reference samples. In order to maximize collection of secondary ions, we explored several instrumental parameters: (i) using $Cs^+$ versus $O^-$ primary ions, (ii) collection of atomic or molecular ions, (iii) primary beam intensity, (iv) dwell time per pixel, (v) raster size and (vi) influence of sample preparation as FIB sections. We subsequently imaged D/H ratios using optimal conditions determined previously in order to maximize the accuracy, sensitivity, precision and reproducibility of D/H ratios at the micrometer-size, while minimizing the surface contamination at the same time. The limit of the method was evaluated by analyzing several NAMs, whose water contents were measured by Elastic Recoil Detection Analysis (ERDA).

## MATERIAL AND METHODS

### Sample preparation

Eight reference samples were used in this study. Two amphiboles spanning a large range of Fe and Mg content (the Bamble Mg-hastingsite and the Illimaussaq Fe-rich arfvedsonite[25], one mica (CRPG phlogopite) and a Mid Ocean Ridge Basaltic glass (DR32[26]) of known water content and H isotopic composition were used (Table S-1) to develop the method and compare matrix effects on FIB sections with classical polished sections. Nominally anhydrous minerals such as Bancroft nepheline and sodalite, 71-98 clinopyroxene and San Carlos olivine were used to monitor contamination during analysis of FIB sections.

All standards were mounted in epoxy stubs polished with SiC disks and diamond paste before being coated with 20 nm Au. Fragments of nepheline and olivine were mounted in indium for comparison with FIB sections and polished section. Having, a hydrogen content lower than 30 ppm $H_2O$ [27], the olivine was used to monitor the background contamination. FIB sections, 2 μm thick and about 5 x 10 μm in area, were extracted from the polished sections of amphiboles, phlogopite and nepheline and deposited onto a polished Al disk, used here to ensure high conductivity and good match with the NanoSIMS sample holders. Another FIB section of 500 nm thickness was extracted from the Illimaussaq amphibole and mounted similarly to determine the erosion rate. In the FIB-Scanning Electron Microscope (FIB-SEM), straps of Pt were deposited at the edges of the FIB sections to anchor them to the Al disk and increase conductivity. All FIB sections were prepared in the FEI strata DB 235 FIB-SEM at IEMN, Lille, France. After deposition, FIB sections were coated with 20 nm Au.

To measure D/H ratios, all samples were introduced in the NanoSIMS airlock between 1 and 21 days before analysis and stored in the vessel chamber in a $10^{-9}$ Torr vacuum in order to monitor the reduction of contamination with time.

### Determination of water content in NAMs

Water content in NAMs (Table S-1) were determined by ERDA using the nuclear microprobe at the Laboratoire d'Etude des Elements Légers, CEA, Saclay, France and following well-established procedures[28,29]. C-coated polished sections of the samples were irradiated using a ~ 3 × 3 μm, 3 MeV, $^4$He beam at a grazing angle yielding a ~ 12 × 3 μm spatial resolution on the samples. Maps were acquired in scanning mode using a 200 μm raster size. Other elements were monitored simultaneously using Rutherford Backscattering and Particle Induced X-ray Emission spectroscopies. Water contents were calculated from the H content obtained from the ERDA spectra and the chemical composition of the samples previously measured at the

CAMPARIS electron microprobe facility in Paris, France in standard analytical conditions. For the considered analytical conditions and studied compositions, ERDA depth of analysis is in the range of 0.5 to 1 μm, leading to spectra with clearly separated hydrogen contributions resulting from surface contamination and bulk content. Uncertainties as indicated in Table S-1 result from counting statistics.

### NanoSIMS Analytical settings

H isotope analyses were performed with the NanoSIMS 50 installed at IMPMC at the Museum National d'Histoire Naturelle in Paris, France using an aperture diaphragm of 750 μm (D1-1), an entrance slit of 50 × 220 μm (ES1), and an aperture slit of 350 × 250 μm (AS1). For all analyses a 20 × 20 μm preanalysis sputtering (hereafter presputtering) was performed during 8 min (5 min on Illimaussaq) with a 250 pA primary beam in order to remove the Au coat and surficial contamination from the analyzed area and to reach sputtering equilibrium. A normal incidence electron flood gun with a beam intensity of 2 μA was used for charge compensation. With this configuration, (i) we first determined, which primary and secondary ions to use in order to maximize the intensity of deuterium. (ii) The $H/^{29}Si$ ratio, a proxy for the water content of the samples[30,31], was subsequently measured on the polished sections to determine the optimal analytical conditions in order to achieve maximal stability together with minimal contamination (Table 1). Finally, (iii) we evaluated the accuracy, precision and reproducibility on the D/H ratio in FIB sections.

We first used a 8 keV $Cs^+$ primary beam and monitored $H^-$ and $^{16}OH^-$ intensities for different primary beam intensities (20 pA, 40 pA, 75 pA, 100 pA, 200 pA, 300 pA and 400 pA). Secondary ion intensities were determined with a default dwell time setting of 132 μs/pixel and 8 μm raster size. $H^+$ ions emitted using 8 keV $O^-$ primary ions from the duoplasmatron source were collected in similar conditions but opposite polarities.

$H^-$ and $^{29}Si^-$ were subsequently collected by magnetic peak jumping on electron multipliers 1 and 5 in order to measure $H/^{29}Si$ ratios using $Cs^+$ primary ions. Optimal analytical conditions were evaluated using six different primary beam intensities (10 pA, 25 pA, 50 pA, 100 pA, 150 pA, 200 pA), five raster sizes (5 μm, 8 μm, 10 μm, 15 μm, 20 μm) and five dwell times (100 μs/px, 300 μs/px, 600 μs/px, 800 μs/px, 1000 μs/px). For each $H/^{29}Si$ measurement, 10 scans of 256 × 256 pixels were acquired for the dwell time of 1000 μs/px. For lower dwell times, the number of scans was adjusted to keep a constant analysis time of about 10 min.

For the measurement of D/H ratios, $H^-$ and $D^-$ were collected in the optimal conditions (Table 1), with simultaneous detection of both isotopes on electron multipliers (EMs) 1 and 2 using a 100 pA primary $Cs^+$ beam, an 8 μm raster and a dwell time of 1000 μs/pixel to form an image of 256 × 256 pixels. 20 scans were acquired for each analysis. In order to remove contamination deposited in the analysis area during the automated measurement of the primary current after presputtering at the beginning of each analysis, the first few cycles were manually removed until $H^-$ intensity was stable[32–34]. Total analysis time is about 20 min. Data were processed with the L'IMAGE software ((c) L. Nittler, 1997). The dead time was set at 44 ns and corrected within L'IMAGE. In order to avoid edge effects associated with a beam size of at most 50 × 50 pixels (Figure S-1), isotope intensities were extracted from a 200 × 200 pixels area. In order to compare and understand instrumental effects, all D/H and H/Si ratios reported here are

raw ratios uncorrected for instrumental fractionation and relative sensitivity factor.

## RESULTS AND DISCUSSION

*Optimal conditions for imaging D/H ratios*

*Choice of primary and secondary ions.* Given the ion yields of hydrogen as secondary ions, hydrogen content and isotopic composition have been measured in SIMS using either H$^-$ and H$^+$ ions[35]. On one hand H$^+$ is known to have a lower yield than H$^-$ [35], but it can be measured without electron gun for charge compensation, which could result in a higher stability and lower contamination if the yield is sufficient. On the other hand, $^{16}$OH$^-$ has a stronger yield than H$^-$ in samples where H is bonded to O (adsorbed or structural water, hydroxyls, H in silicates, phosphates…), so that hydrogen content is also often measured using $^{16}$OH$^-$, especially for samples with low H content[24]. However, the mass resolving power (MRP) required for the measurement of OD$^-$ is much higher (MRP = 8740) than that required to measure D$^-$ or D$^+$ (MRP = 1300), which implies lower intensities for the measurement of D/H ratios. In order to optimize the measurement of FIB sections, we determined on the Bamble amphibole, which of H$^+$, H$^-$ and $^{16}$OH$^-$ gave the highest yield in mass resolution conditions to measure D/H ratios. Figure 1 shows the evolution of H$^+$, H$^-$ and $^{16}$OH$^-$ intensities with primary beam intensity. At the low mass resolving power required to measure D/H ratios using atomic hydrogen, the $^{16}$OH$^-$ intensity is about 15% higher than the H$^-$ intensity, itself higher than H$^+$ intensity by about a factor 2. Given the decrease in $^{16}$OH$^-$ intensity by a factor 3 observed when closing the ES and AS slits to resolve $^{16}$OD$^-$ from the $^{17}$OH$^-$ [22], H$^-$ is the hydrogen ion having the highest yield by far and was subsequently chosen for analysis using Cs$^+$ primary ions.

Figure 1 further shows that above 100-150 pA H$^+$, H$^-$ and $^{16}$OH$^-$ are related with primary beam intensity albeit with a shallower slope than below 100 pA. A likely interpretation is occurrence of charging effects incompletely compensated by the electron gun, which result in a decreased ion yield. Indeed, this decrease in intensity is associated to minor charging effects visible as lines that blur ion images (Figure S-2). As a result, 100 pA is considered in the following as the maximal intensity that can be used in optimal conditions. In negative secondary ion mode, this corresponds to a Cs$^+$ primary beam of ~1.5 µm in diameter.

In the following, the evolution of the H$^-$/$^{29}$Si$^-$ ratio is evaluated as a function of primary beam intensity, raster size and dwell time (Figure 2). The corresponding evolution of the H$^-$ and $^{29}$Si$^-$ secondary ion intensities are given as supplementary Figures S-3 to S-5.
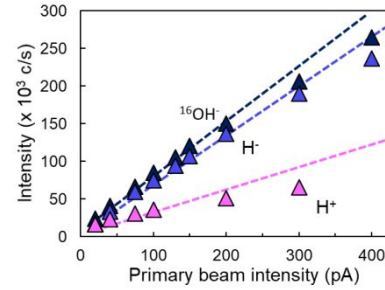


**Figure 1.** Evolution of the intensity of secondary ions with primary beam intensity on Bamble amphibole polished section mounted in epoxy. Cs$^+$ primary beam is used to collect $^{16}$OH$^-$ and H$^-$ ions whereas duo source is used to collect H$^+$ ions. All values are collected in the tuning of the CAMECA software. Dashed lines correspond to the linear relationship between secondary ion intensity and primary beam intensity below 100 pA.

*Effect of primary beam intensity.* The H$^-$/Si$^-$ ratio being a proxy of water content[30,31], some authors used it to track the evolution of contamination against the primary beam intensity[33,34]. They observed that the H$^-$/Si$^-$ ratio decreased with increasing primary beam intensity as a result of a decrease in contamination with increasing primary beam intensity. Stephant et al.[21] studied the evolution of contamination as a function of primary beam intensity using the OH$^-$/Si$^-$ ratio and observed the same trend.

Figure 2a presents the evolution of the H$^-$/$^{29}$Si$^-$ ratio with primary beam intensity, from 20 pA to 200 pA, for a raster width of 8 µm and a dwell time of 1000 µs/px. On both amphiboles, the H$^-$/$^{29}$Si$^-$ ratio decreases when the primary beam intensity increases, reaching a threshold value at 100 pA. While the Bamble amphibole has a constant H$^-$/Si$^-$ ratio above this value, the H$^-$/Si$^-$ is slightly increasing at 150 pA on Illimaussaq due to a decrease in $^{29}$Si intensity, which may be attributed to residual charging effects. At 200 pA, the hydrogen intensity becomes unstable probably due to residual charging, preventing an accurate measurement of the H$^-$/Si$^-$ ratio.

Thus, using a primary beam intensity of 100 pA appears to be a good compromise to limit dynamic contamination, charging effects and have a high hydrogen intensity to measure D/H ratios.
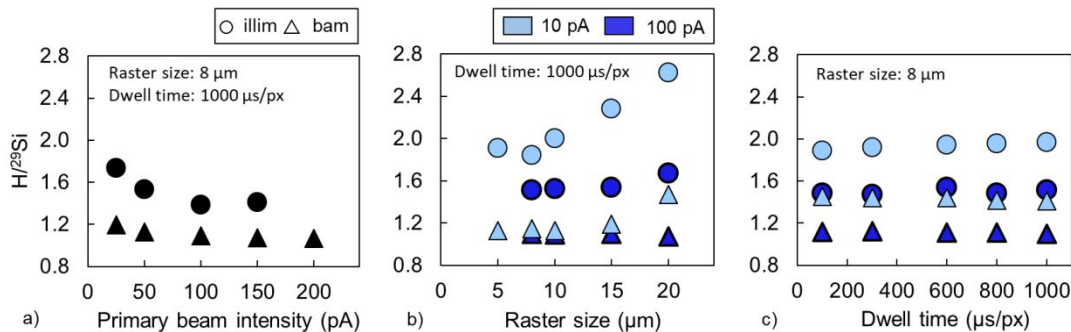


**Figure 2.** Evolution of H/$^{29}$Si ratio of bamble (bam) and illimaussaq (illim) amphiboles with a) primary beam intensity, b) raster size and c) dwell time.
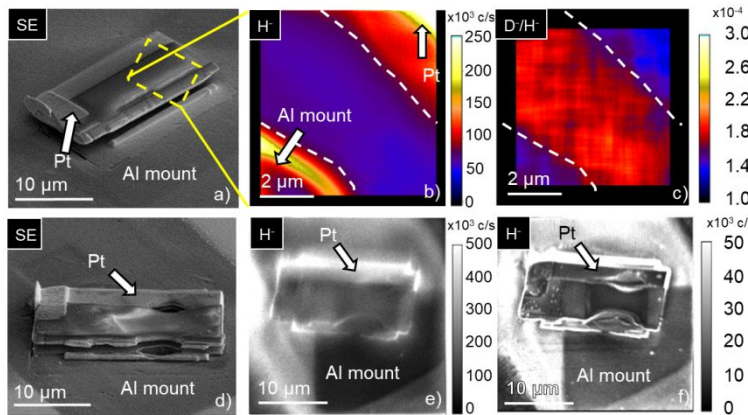
**Figure 3.** a) Secondary electron (SE) image of Bamble amphibole FIB section before NanoSIMS analysis. The square represents the area imaged by NanoSIMS. b) Image of hydrogen secondary ion intensity. c) Corresponding D/H ratio image. d) SE image of Bamble FIB section after NanoSIMS analysis. The darker part on the Al mount next to the FIB section is due to C deposited by the electron beam during the FIB mounting. e) and f) are the ion images of hydrogen of the same FIB section with respectively a primary beam intensity of 100 pA and 10 pA.

*Effect of raster size.* Stephant et al.[21] explored the effect of raster size on dynamic contamination using the $^{16}OH^-/^{28}Si^-$ ratio for primary beam intensities between 1.5 and 15 pA. These authors showed that contamination increases with raster size, and that this increase can be compensated by using a more intense primary beam. Here, we explored the effect of raster size for 10 pA and 100 pA primary intensities and a dwell time of 1000 µs/pixel (Figure 2b).

With a 100 pA primary beam, the $H^-/^{29}Si^-$ ratio decreases on Illimaussaq from 1.67 to 1.54 between 20 µm and 15 µm and is constant between 15 µm and 8 µm. On Bamble, the $H^-/^{29}Si^-$ ratio is constant. We measured $H^-$ and $^{29}Si^-$ intensities for a raster size of 5 µm, but the absence of stability of $H^-$ intensity prevented the measurement of $H^-/^{29}Si^-$ ratio on both amphiboles, probably because a major fraction of the rastered area is affected by edge effects for a large beam and a small raster. By contrast, with a 10 pA primary beam, there is a sharp decrease in the $H^-/^{29}Si^-$ ratio between 20 µm and 10 µm for both amphiboles. Below 10 µm, the $H^-/^{29}Si^-$ ratio is constant.

We thus show that the increase of contamination noticed with increasing raster size[21] is strongly decreased at 100 pA, so that contamination is minimal for a raster size between 15 µm and 8 µm, while raster size should not exceed 10 µm at 10 pA. At 100 pA, the beam size is large, so that the variation in the degree of overlap between adjacent pixels is too small to produce any isotopic effect (the overlap varies between ~90 and 95% when the raster size varies between 8 and 15 µm).

*Effect of dwell time.* Besides raster size, it has been shown that increased dwell time reduced H contamination, notably when primary beam intensity lower than 20 pA were used[21]. Here, we explored the effect of dwell time for a primary beam intensity of 10 pA and 100 pA and a raster size of 8 µm. For samples introduced into vacuum 3 weeks before analysis, no effect of dwell time was observed for both primary beam intensities and both amphiboles (Figure 2c). By contrast, when samples are introduced into vacuum only one week before analysis, there is a sharp decrease in $H^-$ intensity, from $8.4 \times 10^4$ c/s with a dwell time of 100 µs/pixel to $3.4 \times 10^4$ c/s with a dwell time of 1000 µs/pixel (Figure S-6).

As observed before, we show that using large dwell times helps reducing dynamic contamination for incompletely degassed samples. By contrast, extensively degassed samples can be analyzed with any dwell time. We show that allowing for samples to degas in high vacuum (pressure $\leq 10^{-8}$ Torr) during at least 3 weeks prior to analysis results in significant improvement and helps keeping surface contamination negligible compared with the $H^-$ intensity for small raster sizes and high primary beam intensity. Vacuum storage times correspond to the total of pre-analysis storage in the NanoSIMS vessel chamber and residence time in the analysis chamber during week-long analytical sessions, both at ambient temperature. Although pre-analysis sample heating under vacuum should have reduced storage times, common storage of heat sensitive materials in the vessel at the same time for other projects prevented it. Using a primary beam of 100 pA and a raster size between 8 and 15 µm in these conditions allows to minimize both contamination and instabilities due to charging and high sputter rate and provides optimal conditions for imaging D/H ratios.

**Table 1**: Summary of optimal analytical conditions to image H isotopes in weakly hydrated material by NanoSIMS

| | |
|---|---|
| Primary beam intensity | 100 pA |
| Raster size | 8-15 µm |
| Dwell time | 1000 µs/px |
| Pre-analysis vacuum storage time | ~3 weeks |

*Analysis of FIB sections*

*D/H imaging.* Typical images acquired by imaging of H isotopes in optimal conditions in amphibole FIB sections deposited on an Al disk are presented Figure 3. Secondary electron (SE) images acquired before (Figure 3a) and after (Figure 3d) analysis show that the 500 nm thick FIB section is not completely eroded, thus allowing repeated analyses of single FIB sections. The Pt strap deposited on the top part of the sample during FIB sectioning appears to sputter much faster than amphibole. In some cases, this results in a hole in Pt during H isotope imaging (Figure 3d). The SE image further shows that the amphibole is more eroded in contact with Pt due to this enhanced sputtering and along the edges due to topography. Hence, to preserve the FIB section from faster destruction, it is better to minimize the presence of Pt in the image.

With the 100 pA primary beam used during analysis, three zones with different H intensities can usually be identified in FIB section ion images (Figures 3b,d). (i) A central homogeneous zone wich corresponds to $H^-$ from the sample, here amphibole. (ii) A high $H^-$ intensity zone in the border of the section corresponds to the Pt strap. The high emission of $H^-$ in Pt can be explained by its organo-metallic content

corresponding to a C content of about 24 at%[36]. The D/H ratio of H in Pt is significantly lower than that of the amphibole (Figure 3c) most likely due to matrix effects between amphibole and organics. (iii) A zone of varying intensity through time, opposite to the Pt strap, corresponds to the section's edge and the boundary between the amphibole and the Al mount. This boundary shows a high H[-] intensity attributable to topography, which is responsible for creating an angle between the primary beam and the sputtered target surface corresponding to the maximal ion emission[37] instead of the perpendicular angle imposed by the NanoSIMS geometry. We attribute the variable H signal on the Al mount (from $2 \times 10^5$ c/s in the absence of presputtering down to $6 \times 10^3$ c/s) to rapid sputtering of an oxidized/hydrated nm-thick surface layer. Differing intensities around the FIB section can be attributed (Figure 3e,f) to combination in various proportions of enhanced ion emission, where C was deposited by the electron beam in the FIB-SEM during section handling (Figure 3a,d) and decreased ion emission due to sputtering of the oxidized layer during pre-analysis implantation (presputtering). Again the D/H ratio of this surface layer is lower than that of the amphibole (Figure 3c). The high resolution image obtained with a 10 pA primary beam compares well with the secondary electron image in that the H[-] secondary intensity is strongly enhanced with topography and underlines the edges of the section as do secondary electrons (Figure 3f).

*Reduction of static contamination.* Mounting samples as polished sections in epoxy is well-known to result in enhanced H contamination due to degassing / release of atmospheric moisture preferentially adsorbed at the epoxy surface[30,31]. In order to limit the use of epoxy during the sample preparation, Demouchy et al.[38] proposed to mount polished sections in indium. To evaluate the static contamination associated with sample preparation as FIB section, H[-] intensities of Bancroft nepheline prepared as a polished section mounted in epoxy, in indium and as a FIB section were compared for different times after introduction into vacuum (Figure 4a). After 6 days into vacuum, FIB sections appears to be the type of preparation yielding the lowest static contamination with only about $10^4$ c/s H[-]. By contrast, the polished section mounted in epoxy showed the highest H[-] intensity with $9 \times 10^4$ c/s and the polished section mounted in indium yielded and intermediate H[-] count rate of $2.2 \times 10^4$ c/s. After 24 days into vacuum, whatever the preparation used, all count rates are lower than $10^4$ c/s. The decrease of H[-] intensity with time spent in vacuum indicates that a significant fraction of H in the analysis of polished sections is due to surface contamination that is removed by storage at ultra-high vacuum (< $10^{-9}$ Torr). This fraction is especially important for polished sections in epoxy but is also noticeable for preparations in In suggesting it is due to adsorbed atmospheric moisture rather than H degassed from the mount. With a low hydrogen intensity being constant through time, mounting samples as FIB sections appears to be a good way to minimize surface contamination (Figure S-7).

Deloule et al.[35] observed that this decrease in static contamination is associated with an increase in D/H ratios due to a more fractioned D/H ratio (fractionation <<1) in weakly bonded H from contamination. Figure 4b indeed shows that the D/H ratio of the polished section steadily increases from $1.2 \times 10^{-4}$ to $1.8 \times 10^{-4}$ while the D/H ratio of the FIB section is constant through time after introduction into vacuum. These results are in agreement with those obtained on nepheline (Figure 4a): static contamination remains quite important on polished section mounted in epoxy up to 18 days after sample introduction into vacuum, while static contamination is low on FIB sections since the introduction into vacuum. We note that the low D/H ratio of surface contamination during analysis is in line with the low D/H of H in the oxidized surface of the Al mount (Figure 3c).

After 18 days into vacuum, FIB sections and polished sections yielded comparable results for both Bamble and Illimaussaq amphiboles and both 10 pA and 100 pA primary intensities (Figure 4c). Only the first three FIB sections measured at 100 pA show a slightly lower D/H ratio (analyses at 19 and 20 days in Figure 4b, first three FIB sections at 100 pA in Figure 4c). This can be explained by a slight difference in FIB section preparation. Although we systematically used image processing to discount the border of the sections in contact with Pt, contamination by organometallic H with low D/H ratios originating from Pt is still possible during FIB preparation. After these analyses, care was systematically taken to sputter clean the complete surface of the FIB sections using the FIB Ga beam, notably in the lower tilted part of the FIB sections, which resulted in improved D/H ratio consistency between FIB and polished sections.
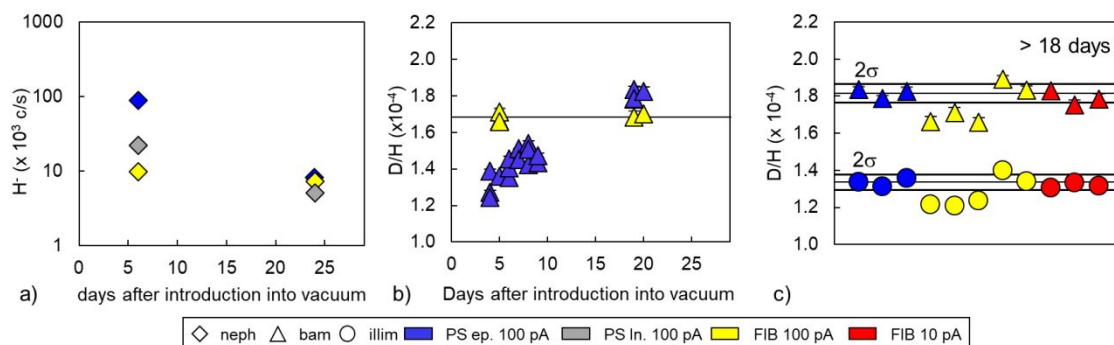


**Figure 4**. a) Evolution of hydrogen intensity of nepheline (neph) prepared as a polished section mounted in epoxy, in indium and as a FIB section. b) D/H ratio evolution with time after introduction of the sample into vacuum of Bamble amphibole FIB section and polished section mounted in epoxy. c) D/H ratio of Bamble (bam) and Illimaussaq (illim) amphibole polished sections mounted in epoxy and FIB section. All data were acquired with a primary beam intensity of 100 pA, except those corresponding to the orange symbols, which were acquired with a primary beam intensity of 10 pA.
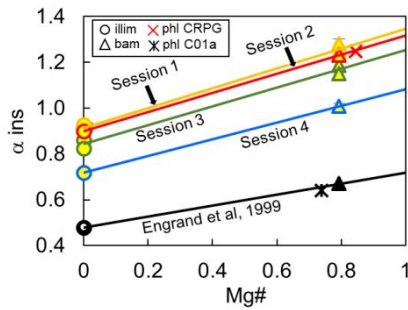
**Figure 5**. Instrumental fractionation factor on FIB sections of Illimaussaq amphibole (illim), Bamble amphibole (bam), and CRPG phlogopite (phl CRPG) during different sessions (represented by different colors). The results acquired by Engrand et al.[34] (shown in black) with an O[-] source, on both amphiboles and phlogopite C01a (phl C01a) are plotted for comparison.

*Matrix effects and reproducibility*. The difference in instrumental fractionation of H isotopes in amphiboles and micas of different chemistry, i.e. the matrix effect, is related to the bonding energy of H with surrounding atoms[35]. In a good approximation, this effect can be corrected using the relationship between fractionation and Mg#, with Mg# defined as $Mg/(Mg+Fe)$[25,35]. Measurements done in four sessions are presented Figure 5. As expected the instrumental fractionation factor varies from session to session, but the linear relationship between fractionation and Mg# remains roughly constant, with a slope of ~0.4, slightly higher but close to the slope of 0.24 obtained by Engrand et al.[25] using an O[-] duoplasmatron source on an IMF 3F instrument. This means that the preparation of FIB sections does not induce an additional matrix effect in comparison with polished sections. For these hydroxylated silicates the instrumental fractionation is still mainly controlled by the electronegativity of the octahedral site[35].

To test the reproducibility of the measurement of D/H ratios by imaging FIB sections, three FIB sections of the Illimaussaq and Bamble amphiboles were measured sequentially. In each image, we defined six circular regions of interest (ROI) of ~1.5 µm of diameter, similar to the size of the 100 pA primary beam and thus corresponding approximately to the lateral resolution of the images (Figure 6). Within a single image, the standard deviation between the ROIs varies from 2.9 x 10^{-6} to 9.9 x 10^{-6} which corresponds to 18 ‰ to 63 ‰ once expressed in per mil deviations relative to the Standard Mean Ocean Water reference value (D/H = $1.5576 \times 10^{-4}$). The typical standard deviation is about $6.2 \times 10^{-6}$ (or ~40 ‰), which compares well with the average Poisson counting statistics (standard deviation = $1/\sqrt{D}$ ≈ 40 ‰, where D is the total number of D counts). Between the bulk FIB sections, the standard deviation is about $2.3 \times 10^{-6}$ (15 ‰), which again compares well with the Poisson statistics. Using the standard error of the mean to evaluate the uncertainties yields similar values (Figure S-8). The overall uncertainty including reproducibility and average counting statistics on bulk FIB section is about $3.3 \times 10^{-6}$ (20 ‰) with 1σ uncertainty.

*Duration of FIB section analysis*. FIB sections are thin and easily destroyed during ion beam sputtering. It is thus essential to determine their erosion rate in order to evaluate the thickness required for an analysis and eventually for multiple analyses including electron microscopy, synchrotron based spectroscopies etc. To measure the erosion rate during typical D/H analyses, a specific FIB section with a thickness of 500 nm was prepared. Two measurements in optimal conditions were made in adjacent craters until the FIB section was totally destroyed. Examination of the images shows that the erosion

can be followed using the intense signal ($\geq 6 \times 10^5$ c/s) that appears when the FIB section is finally eroded (Figures S-9, S10). This signal corresponds to H from the underlying oxidized Al layer no longer protected from sputtering by the FIB section. After sputtering and removal of this surface layer, the edge of the eroded FIB section is visible due to the topographic enhancement of the H intensity. In adjacent craters, erosion starts from the edge of the first crater, which is the thinnest part of the remaining section. For each measurement, the thin FIB section lasted about 30 to 35 minutes (equivalent to a dose of 4.4 to $5.1 \times 10^{19}$ Cs^{+} ions/cm^{2}) and was completely eroded after 40 minutes ($5.9 \times 10^{19}$ Cs^{+} ions/cm^{2}), corresponding to an erosion rate of 0.15 +/- 0.06 nm.µm[2]/pA/s.
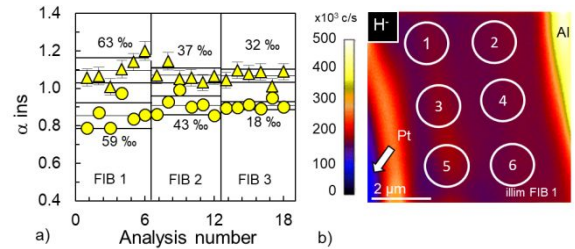


**Figure 6**. a) Instrumental fractionation factor of Illimaussaq (circles) and Bamble (triangles) amphiboles for six regions of interest (ROIs) in three disctinct FIB sections. The standard deviation associated to a FIB section is noted next to the points. b) The hydrogen intensity image of the FIB section 1 of Illimaussaq amphibole is presented with the circular ROIs having a 1.5 µm diameter.

*Sensitivity explored with nominally anhydrous minerals*.

Given the high dynamic range between H and D, a sufficiently high amount of hydrogen must be measured to detect enough deuterium. Two different approaches can be used to estimate the analytical limit for which count rates are too low for a significant determination of the D/H ratios, hence the sensitivity of the method, for both FIB and polished sections.

First, we made the conservative assumption that 1 c/s D[-] or 10 000 c/s H[-] is a reasonable limit to avoid potential problems associated with detector background or count loss due to insufficient signal on individual pixels. Considering this limit the 71-98 clinopyroxene (182 ppm $H_2O$) has H[-] and D[-] count rates too low for a significant measurement, whereas Bancroft nepheline and sodalite (505 and 482 ppm $H_2O$, respectively) have near limit count rates (Figure 7a). By contrast, weakly hydrated phases such as DR32 glass (3099 ppm $H_2O$) and amphiboles (1.6 wt% and 2 wt% $H_2O$) have count rates well above the limit and yield reproducible D/H ratios (Figure 7b).
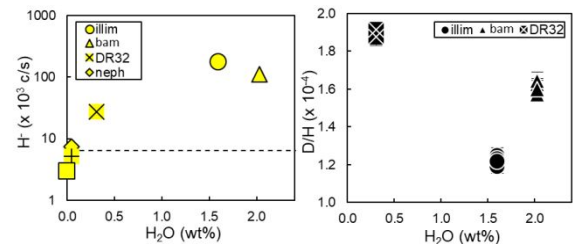


**Figure 7**. a) Hydrogen intensity of minerals prepared as FIB sections as a function of water content. The dashed line represents the hydrogen intensity for which the D count rate is only 1 c/s assuming a D/H ratio equal to the terrestrial reference. b) D/H ratio of minerals prepared as polished section and FIB sections as a function of water content. illim: illimaussaq, bam: bamble, DR32: DR32 glass, neph: nepheline, sod: sodalite, px: 71-98 pyroxene.

Elevated D/H ratios were initially observed in NAMs (Figure S-11) pointing to an analytical artifact at low H count rates. This effect was explored using several polished sections of the San Carlos olivine embedded in epoxy or indium and having spent between 1 day and several months in vacuum to ensure different H count rates on the same sample without changing the analytical conditions (Figure S-11). We found that the observed D/H ratio is highly sensitive to the determination of the optimal ion impact area on the first dynode of the electron multiplier used to count $D^-$ (EM2, Figure 8), which on our instrument appeared to be different from that usually determined for other elements. For low deflector voltages the D/H increases drastically but deflections higher than ~ 80 V yielded consistent D/H ratios. Using a 111 V deflection value, the D/H ratios were found to be comparable in NAMs and amphiboles to the first order (Figure S-11), suggesting that D/H ratios could be measured for count rates below the 1 c/s $D^-$ limit. This optimal deflector voltage was determined for a given EM with a given degree of ageing and should be determined or checked for each analytical session.
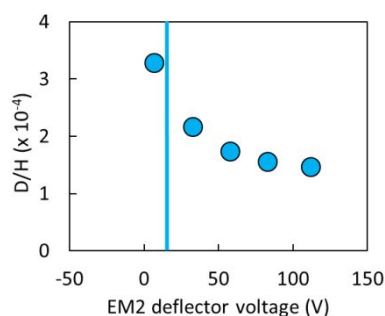


**Figure 8**: D/H ratio measured on San Carlos olivine plotted against the EM2 deflector voltage. The vertical line represents the usual optimal value (12 V).

We determined a very low typical background on EM2 of $2.7 \times 10^{-2}$ c/s, which again suggests that the 1 c/s $D^-$ limit could be too conservative. A more realistic limit to determine the lowest hydrogen concentration for which the D/H ratio can be reasonably measured in NAMs would be an estimate of the surface contamination. The San Carlos olivine (<30 ppm $H_2O$ [27]) used to monitor background hydrogen has an $H^-$ intensity typically about 3000 c/s in optimal conditions. This means that a large part of the signal on NAMs comes from static contamination, thus affecting the measured D/H ratio. With an hydrogen content of ~ 500 ppm and a H count rate around 10000 c/s in nepheline, the background contamination on San Carlos olivine is estimated to 150-200 ppm equivalent $H_2O$, which in our conditions is the lowest limit for analysis of NAMs and introduces a systematic error proportional to its contribution in the total secondary H intensity (e.g. ~30% error for nepheline).

*Applications in geo- and cosmochemistry*

With a typical uncertainty of ~ 50‰ at the 1.5 µm and ~ 20‰ at the bulk FIB section scale and an analytical limit at 200 ppm $H_2O$, the analysis of D/H ratios in FIB sections allows measurement of the composition and heterogeneity of µm-scale minerals, in which significant isotopic variations are expected but where small size and low H content prevented previous analyses.

For instance, the H isotopic composition and potential heterogeneity of the Earth mantle is a key question to decipher the amount and origin of water stored in the deep Earth and to understand the accretion of volatile elements during the formation of our planet. The analysis of olivine-hosted melt inclusions from deeply sourced basalts from Baffin Island and Iceland[39] indeed suggests that these lavas tapped a primordial hidden deep mantle reservoir having a δD value lower than -200 ‰, well below the upper mantle having an average δD around -60 ‰[40], where δD is the D/H ratio given in ‰ deviation relative to the Standard Mean Ocean Water value, the terrestrial reference. A ~40 µm crystal of ringwoodite, a high pressure polymorph of olivine, discovered in inclusion in diamond, was found to contain 1.5 wt% $H_2O$ [41]. This single crystal testifies of a hydrous mantle transition zone between 410 and 660 km. The presently developed method allows H isotope analysis of such rare, small and scientifically precious samples to determine unambiguously the H isotopic composition of deep mantle reservoirs provided the inclusions do not undergo a retrograde transformation changing the solubility of water, upon decompression during sample preparation. At the same time, it allows coupling with other analytical techniques such as TEM or synchrotron-based spectroscopies.

Chondritic meteorites contain high temperature components, the so-called chondrules on one hand and refractory inclusions rich in Ca and Al (CAIs) on the other hand. These components were formed at temperatures $\geq$ 1500 K in the solar protoplanetary disk and constitute the first and major building blocks of terrestrial planets (CAIs and chondrules, respectively). However both often contain secondary minerals indicating more oxidizing conditions than usually expected in the protoplanetary gas. The usual consensus for the origin of these minerals is formation by late hydrothermal circulations on an asteroidal body after accretion[42]. Because astrophysical processes induce large H isotopic heterogeneities, whereas parent-body alteration would tend to homogenize the D/H ratios near the terrestrial composition, the H isotopic composition of these minerals is potentially a good tracer to determine whether oxidizing regions existed in the solar nebula. However these minerals are usually no more than a few µm in size and, apart for rare clay minerals, are usually nominally anhydrous or weekly hydrated minerals with water content lower than 1 wt%, which can now be studied with the present method.

## CONCLUSIONS

This work defines a procedure to measure precisely H isotope ratios on FIB section mounted on an Al substrate and allows subsequent coupling with TEM provided the sections could be recovered and cleaned from the nm-thick layer of ion beam damaged material. It showed that imaging FIB sections provides reproducible and accurate measurements. Using FIB section is additionally a good way to get rid of static contamination without heating the samples. After only 5 days into vacuum, the D/H ratio is constant, whereas about 3 weeks are required for polished sections in epoxy.

In order to image D/H ratio in weakly hydrated materials, the best configuration is to use $H^-$ secondary ions, 100 pA primary intensity, 8 µm raster size and a dwell time of 1000 µs/px. The raster size can be increased up to 15 µm and the dwell time is not a critical parameter given the high primary intensity. In these conditions a precision of a few tens of ‰ can be achieved with a beam size of about 1.5 µm. Finally, the residual background contamination and lowest possible $H_2O$ concentration for H isotope analysis by imaging is estimated to be about 200 ppm.

These analytical developments open new perspectives in the H isotope analysis of small and rare samples, beyond the usual measurement of large isotopic anomalies or isotopically labelled materials.

## AUTHOR INFORMATION

*Corresponding Author*

*Email: dan.levy@mnhn fr

*Notes*

The authors declare no competing financial interest.

## REFERENCES

(1) Slodzian, G.; Daigne, B.; Girard, F.; Hillion, F. Ion Optics for a High Resolution Scanning Ion Microscope and Spectrometer: Transmission Evaluations. *In: Benninghoven, A., Huber, A.M., Werner, H.W. (Eds.), Secondary Ion Mass Spectrometry SIMS IX. Wiley (Chichester)* **1993**, 294–297.

(2) Hillion, F.; Daigne, B.; Girard, F.; Slodzian, G. A New High Performance SIMS Instrument: The Cameca "Nanosims 50". *In: Benninghoven, A., Huber, A.M., Werner, H.W. (Eds.), Secondary Ion Mass Spectrometry SIMS IX. Wiley (Chichester)* **1993**, 254–257.

(3) Carpenter, K. J.; Weber, P. K.; Davisson, M. L.; Pett-Ridge, J.; Haverty, M. I.; Keeling, P. J. Correlated SEM, FIB-SEM, TEM, and NanoSIMS Imaging of Microbes from the Hindgut of a Lower Termite: Methods for In Situ Functional and Ecological Studies of Uncultivable Microbes. *Microscopy and Microanalysis* **2013**, *19* (6), 1490–1501.

(4) Floss, C.; Le Guillou, C.; Brearley, A. Coordinated NanoSIMS and FIB-TEM Analyses of Organic Matter and Associated Matrix Materials in CR3 Chondrites. *Geochimica et Cosmochimica Acta* **2014**, *139*, 1–25.

(5) Groopman, E.; Nittler, L. R.; Bernatowicz, T.; Zinner, E. NanoSIMS, TEM, and XANES Studies of a Unique Presolar Supernova Graphite Grain. *The Astrophysical Journal* **2014**, *790* (1), 9.

(6) Penen, F.; Malherbe, J.; Isaure, M.-P.; Dobritzsch, D.; Bertalan, I.; Gontier, E.; Le Coustumer, P.; Schaumlöffel, D. Chemical Bioimaging for the Subcellular Localization of Trace Elements by High Contrast TEM, TEM/X-EDS, and NanoSIMS. *Journal of Trace Elements in Medicine and Biology* **2016**, *37*, 62–68.

(7) Le Guillou, C.; Remusat, L.; Bernard, S.; Brearley, A. J.; Leroux, H. Amorphization and D/H Fractionation of Kerogens during Experimental Electron Irradiation: Comparison with Chondritic Organic Matter. *Icarus* **2013**, *226* (1), 101–110.

(8) Suer, T.-A.; Siebert, J.; Remusat, L.; Menguy, N.; Fiquet, G. A Sulfur-Poor Terrestrial Core Inferred from Metal–Silicate Partitioning Experiments. *Earth and Planetary Science Letters* **2017**, *469*, 84–97.

(9) DeNiro, M. J.; Epstein, S. Hydrogen Isotope Ratios of Mouse Tissues Are Influenced by a Variety of Factors Other than Diet. *Science* **1981**, *214* (4527), 1374–1376.

(10) Hobson, K. A.; Atwell, L.; Wassenaar, L. I. Influence of Drinking Water and Diet on the Stable-Hydrogen Isotope Ratios of Animal Tissues. *Proceedings of the National Academy of Sciences* **1999**, *96* (14), 8003–8006.

(11) Craig, H. Isotopic Variations in Meteoric Waters. *Science* **1961**, *133* (3465), 1702–1703.

(12) Dansgaard, W. Stable Isotopes in Precipitation. *Tellus* **1964**, *16* (4), 436–468.

(13) Lécuyer, C.; Gillet, P.; Robert, F. The Hydrogen Isotope Composition of Seawater and the Global Water Cycle. *Chemical Geology* **1998**, *145* (3), 249–261.

(14) Zinner, E.; McKeegan, K. D.; Walker, R. M. Laboratory Measurements of D/H Ratios in Interplanetary Dust. *Nature* **1983**, *305* (5930), 119–121.

(15) Messenger, S. Identification of Molecular-Cloud Material in Interplanetary Dust Particles. *Nature* **2000**, *404* (6781), 968.

(16) Altwegg, K.; Balsiger, H.; Bar-Nun, A.; Berthelier, J. J.; Bieler, A.; Bochsler, P.; Briois, C.; Calmonte, U.; Combi, M.; De Keyser, J.; et al. 67P/Churyumov-Gerasimenko, a Jupiter Family Comet with a High D/H Ratio. *Science* **2015**, *347* (6220), 1261952–1261952;

(17) Robert, F.; Merlivat, L.; Javoy, M. Deuterium Concentration in the Early Solar System: Hydrogen and Oxygen Isotope Study. *Nature* **1979**, *282* (5741), 785–789.

(18) Sternberg, L. da S. L. D/H Ratios of Environmental Water Recorded by D/H Ratios of Plant Lipids. *Nature* **1988**, *333* (6168), 59.

(19) Jacob, J.; Huang, Y.; Disnar, J.-R.; Sifeddine, A.; Boussafir, M.; Spadano Albuquerque, A. L.; Turcq, B. Paleohydrological Changes during the Last Deglaciation in Northern Brazil. *Quaternary Science Reviews* **2007**, *26* (7), 1004–1015.

(20) Magee, C. W.; Botnick, E. m. Hydrogen Depth Profiling Using SIMS—Problems and Their Solutions. *Journal of Vacuum Science and Technology* **1981**, *19* (1), 47–52.

(21) Stephant, A.; Remusat, L.; Thomen, A.; Robert, F. Reduction of OH Contamination in Quantification of Water Contents Using NanoSIMS Imaging. *Chemical Geology* **2014**, *380*, 20–26.

(22) Piani, L.; Remusat, L.; Robert, F. Determination of the H Isotopic Composition of Individual Components in Fine-Scale Mixtures of Organic Matter and Phyllosilicates with the Nanoscale Secondary Ion Mass Spectrometry. *Anal. Chem.* **2012**, *84* (23), 10199–10206.

(23) Piani, L.; Robert, F.; Remusat, L. Micron-Scale D/H Heterogeneity in Chondrite Matrices: A Signature of the Pristine Solar System Water? *Earth and Planetary Science Letters* **2015**, *415*, 154–164.

(24) Novella, D.; Frost, D. J.; Hauri, E. H.; Bureau, H.; Raepsaet, C.; Roberge, M. The Distribution of H2O between Silicate Melt and Nominally Anhydrous Peridotite and the Onset of Hydrous Melting in the Deep Upper Mantle. *Earth and Planetary Science Letters* **2014**, *400*, 1–13.

(25) Engrand, C.; DeLoule, E.; Robert, F.; Maurette, M.; Kurat, G. Extraterrestrial Water in Micrometeorites and Cosmic Spherules from Antarctica: An Ion Microprobe Study. *Meteoritics & Planetary Science* **1999**, *34* (5), 773–786.

(26) Clog, M. Concentration et Composition Isotopique En Hydrogène Du Manteau Terrestre. thesis, Paris 7, 2010.

(27) Chen, J.; Liu, H.; Girard, J. Comparative in Situ X-Ray Diffraction Study of San Carlos Olivine: Influence of Water on the 410 Km Seismic Velocity Jump in Earth's Mantle. *American Mineralogist* **2011**, *96* (5–6), 697–702.

(28) Bureau, H.; Raepsaet, C.; Khodja, H.; Carraro, A.; Aubaud, C. Determination of Hydrogen Content in Geological Samples Using Elastic Recoil Detection Analysis (ERDA). *Geochimica et Cosmochimica Acta* **2009**, *73* (11), 3311–3322.

(29) Withers, A. C.; Bureau, H.; Raepsaet, C.; Hirschmann, M. M. Calibration of Infrared Spectroscopy by Elastic Recoil Detection Analysis of H in Synthetic Olivine. *Chemical Geology* **2012**, *334*, 92–98.

(30) Hauri, E.; Wang, J.; Dixon, J. E.; King, P. L.; Mandeville, C.; Newman, S. SIMS Analysis of Volatiles in Silicate Glasses 1. Calibration, Matrix Effects and Comparisons with FTIR. *Chemical Geology* **2002**, 16.

(31) Koga, K.; Hauri, E.; Hirschmann, M.; Bell, D. Hydrogen Concentration Analyses Using SIMS and FTIR: Comparison and Calibration for Nominally Anhydrous Minerals. *Geochemistry, Geophysics, Geosystems* **2003**, *4* (2).

(32) Wittmaack, K. Background Formation in SIMS Analysis of Hydrogen, Carbon, Nitrogen and Oxygen in Silicon. *Nuclear Instruments and Methods in Physics Research* **1983**, *218* (1–3), 327–332.

(33) Rhede, D.; Wiedenbeck, M. SIMS Quantification of Very Low Hydrogen Contents. *Applied Surface Science* **2006**, *252* (19), 7152–7154.

(34) Ludwig, T.; Stalder, R. A New Method to Eliminate the Influence of in Situ Contamination in SIMS Analysis of Hydrogen. *J. Anal. At. Spectrom.* **2007**, *22* (11), 1415–1419.

(35) Deloule, E.; France-Lanord, C.; Albarède, F. D/H Analysis of Minerals by Ion Probe. *the Geochemical society* **1991**, No. 3, 53–62.

(36) Tao, T.; Ro, J.; Melngailis, J.; Xue, Z.; Kaesz, H. D. Focused Ion Beam Induced Deposition of Platinum. *Journal of Vacuum Science & Technology B: Microelectronics Processing and Phenomena* **1990**, *8* (6), 1826–1829.

(37) Blanchard, B. Analyse Par Émission Ionique Secondaire SIMS. *Techniques de l'ingénieur* **1988**.

(38) Demouchy, S.; Deloule, E.; Frost, D. J.; Keppler, H. Pressure and Temperature-Dependence of Water Solubility in Fe-Free Wadsleyite. *American Mineralogist* **2005**, *90* (7), 1084–1091.

(39) Hallis, L. J.; Huss, G. R.; Nagashima, K.; Taylor, G. J.; Halldórsson, S. A.; Hilton, D. R.; Mottl, M. J.; Meech, K. J. Evidence for Primordial Water in Earth's Deep Mantle. *Science* **2015**, *350* (6262), 795–797.

(40) Clog, M.; Aubaud, C.; Cartigny, P.; Dosso, L. The Hydrogen Isotopic Composition and Water Content of Southern Pacific MORB: A Reassessment of the D/H Ratio of the Depleted Mantle Reservoir. *Earth and Planetary Science Letters* **2013**, *381*, 156–165.

(41) Pearson, D. G.; Brenker, F. E.; Nestola, F.; McNeill, J.; Nasdala, L.; Hutchison, M. T.; Matveev, S.; Mather, K.; Silversmit, G.; Schmitz, S.; et al. Hydrous Mantle Transition Zone Indicated by Ringwoodite Included within Diamond. *Nature* **2014**, *507* (7491), 221–224.

(42) Brearley, A. J.; Krot, A. N. Metasomatism in Chondritic Meteorites. In 'Metasomatism and the Chemical Transformation of Rock: The Role of Fluids in Terrestrial and Extraterrestrial Processes' Lecture Notes in Earth Sciences Series; Springer, 2013; pp 653–782.